Optical Absorption Tomography for Carbon Dioxide Concentration Imaging

Optical Absorption Tomography for Carbon Dioxide Concentration Imaging

N Polydorides[1], E Fisher[1], A Tsekenis[1], L Dimiccoli[2] and H McCann[1]

[1]School of Engineering, University of Edinburgh, Edinburgh, UK

[2]Department of Electronics and Informatics, Vrije University of Brussels, Belgium.

E-mail: n.polydorides@ed.ac.uk

Abstract. We consider the inverse problem of concentration imaging in chemical species tomography with limited data sets. The measurement setup involves simultaneous acquisition of near infrared wavelength-modulated spectroscopic measurements from a small number of pencil beams equally distributed among six projection angles surrounding the plume. We develop an approach for image reconstruction that involves constraining the value of the image to the conventional concentration bounds and a projection into low-dimensional subspaces to reduce the degrees of freedom in the inverse problem. We impose three types of inequality constraints, namely positivity, boundedness and logarithmic boundedness in a simple and elegant way that yields an unconstrained optimisation problem in a new set of surrogate parameters. Testing this numerical scheme with simulated and controlled experimental data indicates that the combination of affine inequality constraints and subspace projection leads to images that are qualitatively and quantitatively superior in spatial resolution to Tikhonov-based reconstructions. This improvement is more profound in targeting concentration profiles with small variation. We present images and convergence graphs from solving these inverse problems using Gauss-Newton's algorithm to demonstrate the performance and convergence of our method.

1. Introduction

We consider the inverse problem in chemical species tomography (CST) for reconstructing the concentration image x from the discrete linear attenuation model

$$y = Ax + \epsilon, \tag{1}$$

where $A \in \mathbb{R}^{m\times n}$ is the discretized measurement operator and ϵ is additive zero-mean noise. We are interested in the situations where the degrees of freedom n in the sought image exceeds by far the number of available data m, as this tends to be the conventional setting in CST measurements [1]. For $m \ll n$ the underdetermined model (1) attains a large null space and thus admits infinite, invariably different solutions, making the reconstruction of the true concentration problematic with limited data sets. To rectify the situation one typically applies some form of regularisation, usually of a Tikhonov-type [2], that stabilises the inversion process and yields imaging with adequate resolution but when n is large it becomes computationally expensive, and challenging to optimise.

Our approach seeks to enforce some affine inequality constraints on the image so that to bound the concentration to its default admissible range, as well reducing the dimension of the parameter space by projecting the image onto a subspace of basis functions that are consistent

with its expected features. The methodology we propose has two distinct phases: We first model the concentration using a family of surrogate functions and parameters and then we formulate the inverse problem with respect to these new set of parameters projected onto the low-dimensional subspace. This provides an elegant way to impose affine inequality constraints and reduce the dimensionality of the inverse problem, transforming it into a small unconstrained optimisation problem for a convex-differentiable cost function. The appeal of this approach lies in its simplicity of implementation and computational robustness, although other constrained convex optimisation algorithms, such as the projected gradients algorithms [3], active sets [4], interior point methods [5] or through sequential unconstrained programming using penalty and barrier formulations [6], are also suitable to the task.

We describe our methodology beginning with some important definitions. The subspace of bounded vectors in $\mathcal{S}_1 \subset \mathbb{R}^n$

$$\mathcal{S}_1 \doteq \{x \in \mathbb{R}^n \mid \ell \leq x \leq u\}, \quad \text{where} \quad 0 < \ell < u, \tag{2}$$

for some finite bounds ℓ and u. Further let a continuous and invertible, one-to-one mapping $\upsilon : \mathbb{R}^n \to \mathcal{S}_1$. Then there exists a unique vector of unconstrained parameters $\rho \in \mathbb{R}^n$ such that

$$x = \upsilon(\rho), \quad \forall x \in \mathcal{S}_1. \tag{3}$$

We aim to compute the projection of the high-dimensional ρ in a low-dimensional space of basis functions $\mathcal{S}_2 \subset \mathbb{R}^n$, such that

$$\mathcal{S}_2 \doteq \{\Phi r \mid r \in \mathbb{R}^s\}, \tag{4}$$

where $\Phi \in \mathbb{R}^{n \times s}$ is a matrix whose columns form an orthonormal basis of some feature functions $\{\phi_1, \ldots, \phi_s\}$ with $s \ll n$. This arrangement allows to formulate an inverse problem for the projection of the unconstrained vector of parameters ρ in $\mathcal{S}_2$, from which we ultimately obtain a constrained concentration image

$$\hat{x} = \upsilon(\Pi\hat{\rho}), \quad \text{where} \quad \Pi\rho = \Phi\rho, \tag{5}$$

for $\Pi : \mathbb{R}^n \to \mathcal{S}_2$ the associated projection matrix operator. This framework enforces affine inequality constraints on the admissible range of the image while it approximates the solution within a subspace of basis functions that are consistent with the expected features of the concentration image. For the targeted CST application the benefit of this approach is twofold. It constrains the concentration image within its intrinsic bounds 0 – 100%, and thereafter it allows to formulate the inverse problem for the logarithm of the concentration and thus making it more suitable to image low-contrast concentration plumes. In the next section we present the foundation of our approach, namely the use of nonlinear surrogate functions that are suitable to model the constraints on the concentration image.

2. Surrogate functions

For a fixed $\mathcal{S}_1$, we can find a reparameterisation of $x \in \mathcal{S}_1$ via an invertible and analytic mapping

$$\upsilon : \mathbb{R} \to \mathcal{S}_1 \tag{6}$$

that we name the surrogate mapping. The invertibility provides υ with the simultaneous surjectivity and injectivity, whereas the analyticity provides υ with infinite differentiability. The most simple and practical manner to insure invertibility consists in considering mappings that are strictly monotonic.

We describe a practical method that can be used to obtain a surrogate mapping. We focus initially on a surrogate mapping that satisfies the strict positiveness of the concentration. Thereafter, we show how we can reuse this surrogate mapping in order to obtain another surrogate mapping that bounds x or its logarithm between two strictly positive bounds.

2.1. Strict positiveness.
If $\mathcal{S}_1$ is the set of the real numbers that are larger than a real number $\ell > 0$ then the following invertible and analytic function

$$\upsilon_{\mathrm{p}}(\rho;\ell) \doteq \mathrm{e}^{\rho} + \ell, \quad \forall\ \rho \in \mathbb{R},$$

is a model of the surrogate mapping (6). In particular, $\upsilon_{\mathrm{p}}(\rho;0)$ is the inverse of the logarithmic function that has already been proposed as a model of the inverse mapping of (6) [7].

2.2. Boundedness.
Consider the following function

$$\upsilon_{\mathrm{s}}(\rho;\ell,u) \doteq \ell + \frac{u-\ell}{1+\rho^{-1}}, \quad \forall\ \rho \in \mathbb{R},\ \forall\ \ell,u \in \mathbb{R},\ \ell < u.$$

If $\mathcal{S}_1$ is the set of the real numbers in the open interval of endpoints ℓ and u, with $0 < \ell$, then for a real number q such that $0 \leq q \leq u$ we can define the following invertible and analytic function

$$\upsilon_{\mathrm{b}}(\rho;\ell,q,u) \doteq \upsilon_{\mathrm{s}}(\upsilon_{\mathrm{p}}(\rho;\ell-q);\ell,u) = \ell + \frac{u-\ell}{1+(\mathrm{e}^{\rho}+\ell-q)^{-1}}, \quad \forall\ \rho \in \mathbb{R}, \tag{7}$$

so that the following function

$$\upsilon_{\mathrm{b}}(\rho;\ell,\ell,u) = \ell + \frac{u-\ell}{1+\mathrm{e}^{-\rho}}, \quad \forall\ \rho \in \mathbb{R},$$

thus υ_{b} is just another expression of a model of (6).

2.3. Logarithmic boundedness.
A particular case of boundedness occurs when we consider x in an interval that is spanning over several orders of magnitude, or when the interval is extremely narrow. In such cases, it is more appropriate to bound the logarithm of x. Indeed by noting that

$$\mathrm{e}^{\ell} < x < \mathrm{e}^{u} \iff \ell < \log x < u,$$

then by using a function

$$\upsilon_{\mathrm{l}}(\rho) \doteq \log \rho, \quad \forall\ \rho \in \mathbb{R},\ \text{s.t. } \rho > 0,$$

and the mapping υ_{p} described in section 2.1, we can relate the boundedness of $\log x$ to the ordinary boundedness described in section 2.2. For $\rho = \log x$ it follows that $\rho = \upsilon_{\mathrm{l}}(\upsilon_{\mathrm{p}}(\rho;0))$ and thus

$$\upsilon_{\mathrm{l}} \circ \upsilon_{\mathrm{p}} : \log x \mapsto \upsilon_{\mathrm{b}}(\rho;\ell,\ell,u).$$

Note that if $\mathcal{S}_1$ is the set of the real numbers that are strictly positive and whose logarithm is in the open interval with endpoints ℓ and u, then $\upsilon_{\mathrm{b}}(\rho;\ell,\ell,u)$ is not a model of the surrogate mapping (6), because υ_{b} maps $\rho \in \mathbb{R}$ to $\log x$ instead of x. However, since the range of $\upsilon_{\mathrm{b}}(\rho;\ell,\ell,u)$ is the interval with endpoints ℓ and u, since x can be obtained from υ_{b} univocally, then

$$\upsilon_{\mathrm{p}}(\upsilon_{\mathrm{b}}(\rho;\ell,\ell,u);0)$$

always maps x onto $\mathcal{S}_1$, and it is just another expression of a model of (6).

2.4. Generic surrogate mapping.
According to the constraints applied on x, using the invertible and analytic mappings described in section 2.1-2.3, we can define a model of the surrogate mapping (6) as follows:

$$x = \upsilon(\rho) \doteq \begin{cases} \upsilon_{\mathrm{p}}(\rho;\ell) & \text{if } \mathcal{S}_1 = \{x \in \mathbb{R}^n \,|\, 0 < \ell < x\} \quad (8a) \\ \upsilon_{\mathrm{b}}(\rho;\ell,\ell,u) & \text{if } \mathcal{S}_1 = \{x \in \mathbb{R}^n \,|\, 0 < \ell < x < u\} \quad (8b) \\ \upsilon_{\mathrm{p}}(\upsilon_{\mathrm{b}}(\rho;\ell,\ell,u);0) & \text{if } \mathcal{S}_1 = \{x \in \mathbb{R}^n \,|\, 0 < x,\ \ell < \log x < u\} \quad (8c) \end{cases}$$

Notice that (8a) is a special case of (8b). Indeed, if in (7) we replace υ_{s} with the identity mapping $\mathrm{id}(\upsilon_{\mathrm{p}}) = \upsilon_{\mathrm{p}}$ then $\upsilon_{\mathrm{b}}(\rho;\ell,0,u) = \upsilon_{\mathrm{p}}(\rho;\ell)$. Similarly, (8b) is a special case of (8c). Indeed, if $0 < \ell$ and we replace $\log x$ and υ_{p} respectively with x and the identity mapping $\mathrm{id}(\upsilon_{\mathrm{b}}) = \upsilon_{\mathrm{b}}$ then $\upsilon_{\mathrm{p}}(\upsilon_{\mathrm{b}}(\rho;\ell,\ell,u);0) = \upsilon_{\mathrm{b}}(\rho;\ell,\ell,u)$. For this reason, we can obtain the derivatives of υ by considering only the derivatives of (8c). To keep the notation as general as possible, for all $x \in \mathcal{S}_1$ and $\rho \in \mathbb{R}^n$ we have

$$x = \Upsilon(\rho) = [\Upsilon_j(\rho)]_{j=1}^n, \quad \Upsilon_j(\rho) \doteq \upsilon(\rho_j), \tag{9}$$

and we notice that if $n = 1$ then Υ reduces to υ. The Jacobian matrix of Υ is then shown to be

$$\mathrm{J}\Upsilon(\rho) = \mathrm{D}\left[\frac{\mathrm{d}}{\mathrm{d}\rho_j}\upsilon(\rho_j)\right]_{j=1}^n, \tag{10}$$

where D is an operator that transforms a vector ρ in the diagonal matrix whose main diagonal equals ρ. By applying the chain rule of differentiation on (8c) we obtain that

$$\begin{aligned} \frac{\mathrm{d}}{\mathrm{d}\rho_j}\upsilon(\rho_j) &= \frac{\mathrm{d}}{\mathrm{d}\upsilon_{\mathrm{b}}}\upsilon_{\mathrm{p}}(\upsilon_{\mathrm{b}}(\rho_j;\ell,\ell,u);0)\frac{\mathrm{d}}{\mathrm{d}\upsilon_{\mathrm{p}}}\upsilon_{\mathrm{s}}(\upsilon_{\mathrm{p}}(\rho_j;0);\ell,u)\frac{\mathrm{d}}{\mathrm{d}\rho_j}\upsilon_{\mathrm{p}}(\rho_j;0) \\ &= \frac{\upsilon_{\mathrm{p}}(\upsilon_{\mathrm{b}}(\rho_j;\ell,\ell,u);0)(u-\ell)\upsilon_{\mathrm{p}}(\rho_j;0)}{(1+\upsilon_{\mathrm{p}}(\rho_j;0))^2}, \end{aligned}$$

therefore in general the derivative of υ is

$$\frac{\mathrm{d}}{\mathrm{d}\rho_j}\upsilon(\rho_j) = \begin{cases} \upsilon_{\mathrm{p}}(\rho_j;0) & \text{if (8a)} \\ \frac{(u-\ell)\,\upsilon_{\mathrm{p}}(\rho_j;0)}{(1+\upsilon_{\mathrm{p}}(\rho_j;0))^2} & \text{if (8b)} \\ \frac{\upsilon(\rho_j)\,(u-\ell)\,\upsilon_{\mathrm{p}}(\rho_j;0)}{(1+\upsilon_{\mathrm{p}}(\rho_j;0))^2} & \text{if (8c)} \end{cases}. \tag{11}$$

3. The projected inverse problem

Having defined the surrogate functions for the concentration image we set out to cast the inverse problem with respect to the surrogate parameters ρ. To stabilise the inversion we reduce the degrees of freedom in the resulting inverse problem, by adopting the following assumption. If we consider a projection $\Pi\rho \in \mathcal{S}_2$ then we seek to reconstruct x when its corresponding surrogate image $\rho = \upsilon^{-1}(x)$ satisfies

$$\frac{\|\rho - \Pi\rho\|}{\|\rho\|} < w < 1,$$

since ultimately our approach is restricted to reconstructing only the $\Pi\rho$ of x. The choice of basis functions Φ involved in the projection $\Pi = \Phi(\Phi^T\Phi)^{-1}\Phi^T$ is made to impart some level of smoothness to the expected image, as this is consistent with the expected profile of the concentration and plume velocity. From the surrogate form of model (1),

$$y = A\upsilon(\rho) + \epsilon, \tag{12}$$

linearising at point $\rho^{(i)}$ yields

$$y \approx A\big(\upsilon(\rho^{(i)}) + \mathrm{J}\Upsilon(\rho^{(i)})(\rho - \rho^{(i)})\big) + \epsilon,$$

and thus imposing $\Pi\rho = \Phi r$ and setting $y(\rho^{(i)}) = y - A\upsilon(\rho^{(i)}) + A\mathrm{J}\Upsilon(\rho^{(i)})\rho^{(i)}$ and $K(\rho^{(i)}) = A\mathrm{J}\Upsilon(\rho^{(i)})$, we arrive at the ith projected surrogate model

$$y(\rho^{(i)}) = K(\rho^{(i)})\Phi r + \tilde{\epsilon}, \tag{13}$$

with the noise $\tilde{\epsilon}$ now including also the projection approximation error. In the context of the Gauss-Newton algorithm, an image can be reconstructed iteratively by solving the regularised problems

$$\hat{r}^{(i+1)} = \underset{r\in\mathbb{R}^s}{\operatorname{argmin}}\Big\{ \big\|y(\rho^{(i)}) - K(\rho^{(i)})\Phi r\big\|^2 + \lambda^2\big\|r - r^{(i)}\|^2\Big\}, \quad i = 1, 2, \ldots, \tag{14}$$

where λ is a regularisation parameter, $\rho^{(i)} = \Phi r^{(i)}$, and the Jacobian of υ can be obtained from the formulas (8a)-(8c). The progress of the iterations is governed by Morozov's discrepancy principle, while the value of λ can be adjusted as shown in [1]. Ultimately, the reconstructed concentration image can be obtained from (14) by $\hat{x}^{(i)} = \upsilon(\Phi\hat{r}^{(i)})$.

4. Numerical results

In this section we present some results obtained from numerical simulation experiments. Data were computed from (1) based a high resolution grid with $n = 10000$ elements for a target concentration image x and then infused with zero-mean Gaussian noise with variance of 1% of the mean data value. The bounds for the true concentration were at $3\times10^{-4} \le x \le 1$ and for this test we have used a subspace of 225 radial basis functions, orthonormalised through the Gram-Schmidt process [8]. In turn this led to a projection approximation error of $\|\rho - \Pi\rho\|/\|\rho\| \approx 0.12$ which forms the lower bound of the image reconstruction error. We run the algorithm described in the previous section for the three types of surrogate mappings and compare the results with that obtained from the Tikhonov solution

$$\hat{x}_t = (A^TA + \lambda^2R^TR)^{-1}(A^Ty + \lambda^2R^TRx_0), \tag{15}$$

for a smoothness imposing regularisation matrix $R \in \mathbb{R}^{n\times n}$ and a uniform prior guess x_0. These simulations we computed with a scaled-down version of the data model having $n = 4900$ parameters on which we have also approximated the targeted concentration to aid comparison in the reconstructions. The images, which are presented in figure 1, show that the performance of our scheme exceeds that of Tikhonov method, which yields irrational negative concentration values. The results correspond to running 10 Gauss-Newton iterations on the projected inverse problem for the surrogate parameters with λ fixed at 10^{-2}. In this 'high-variation' benchmark test the three surrogate formulations perform almost equally well, converging to a solution after the first 8 iterations as shown in figure 3. The Tikhonov solution with the same data and $\lambda = 1$ attains a smaller data error at 7×10^{-3} but the error in the image is higher. To make the comparison objective all initial prior guess images were chosen to be positive and homogenous.

To investigate the situation of low variation concentration we repeat the simulations on a similar phantom but the concentration levels are adjusted to the range $1.51 \times 10^{-5} \le x \le 0.16$ as shown in figure 2. In this setting we repeat the simulations using the same values of λ and number of iterations and have obtained the images illustrated in figure 2 and the convergence plots in the right hand side of figure 3. In consistency with the 'high-variation' results our methodology seems to perform better than the smoothness imposing Tikhonov regularisation,

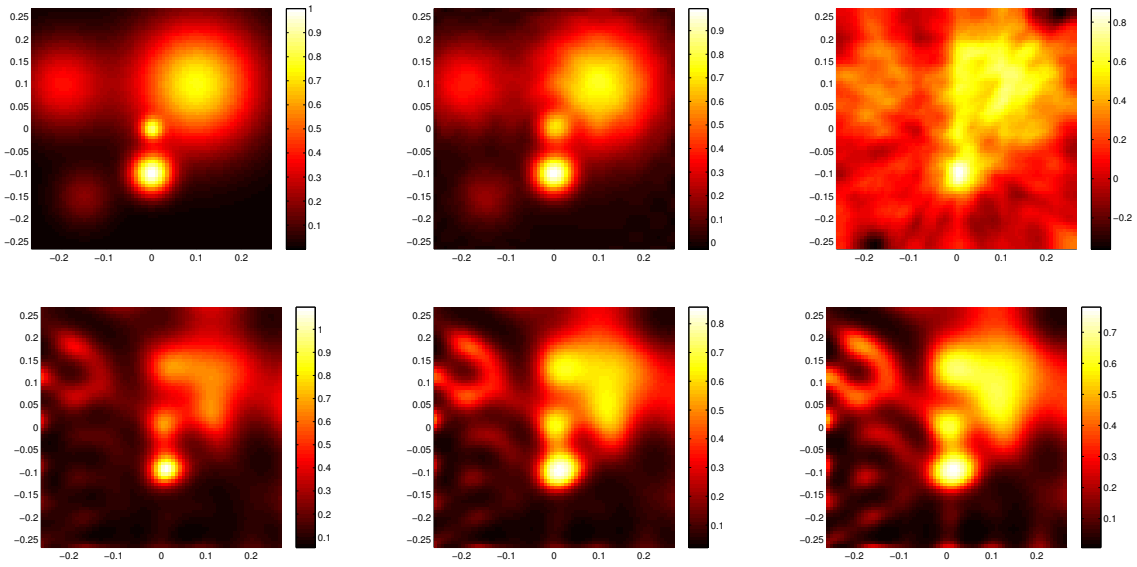

Figure 1. At the top row the high-variation target image x in a 70×70 square grid, its projection $\Pi\rho$ on the same grid, and the Tikhonov solution. Below, the images after 10 Gauss-Newton iterations based on with positiveness, boundedness and logarithmic boundedness surrogate functions.

even when the subspace projection error is larger, see for example the discrepancy between the images of the target $v(\rho)$ (on the coarser grid) and its subspace projection $\Pi\rho$ in figure 2. This set of results reveals also that in this case bounding the values of the image or indeed the logarithm of the image improves the reconstruction, both in terms of the spatial resolution of the images but also in terms of the convergence of the reconstruction algorithm.

5. Real data reconstruction

In this section we present some reconstructions from measurements captured from phantom experiments using the FLITES instrumentation system [1]. The data correspond to two circular, homogenous Carbon dioxide plumes arranged diagonally with the computational domain, one at 40 cm diameter and the other at 60 cm. The concentration of the gas we set to about 6% for both plumes. In the image reconstruction we have used the same surrogate formulations as above, although in this case we have projected the surrogate problem into a basis of 64 discrete cosine basis functions. The results are plotted in figure 4 were obtained after 4 iterations of the Gauss-Newton algorithm for the three different surrogate formulations at a relative data error of around 0.6. Compared to the smooth Tikhonov image, the iterative results appear to be quantitatively and qualitatively superior. Unfortunately, the difference in the diameter of the two plumes is less profound in these images.

6. Conclusions

We presented an algorithmic framework for solving the chemical species concentration tomography problem with affine inequality constraints. The key aspect of our approach is the use of surrogate functions that model the affine constraints and transform the constrained inverse problem into an unconstrained one. To cope with the shortage of data the problem was subsequently projected onto a low-dimensional basis of interpolation functions. The resulting

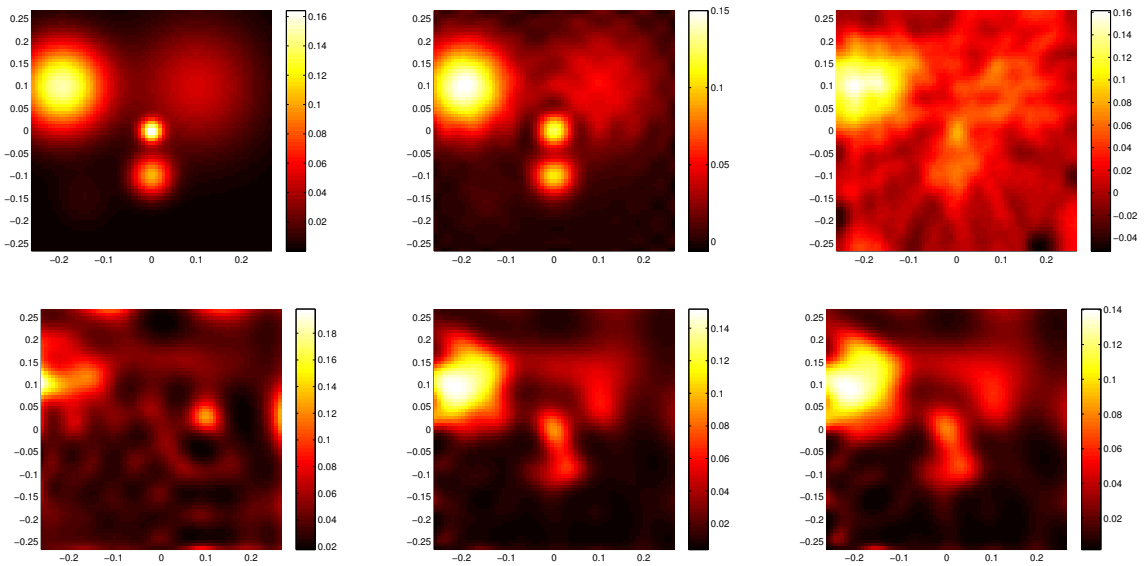

Figure 2. At the top row the low-variation target image x in a 70×70 square grid, its projection $\Pi\rho$ on the same grid, and the Tikhonov solution. Below, the images after 10 Gauss-Newton iterations based on with positiveness, boundedness and logarithmic boundedness surrogate functions.

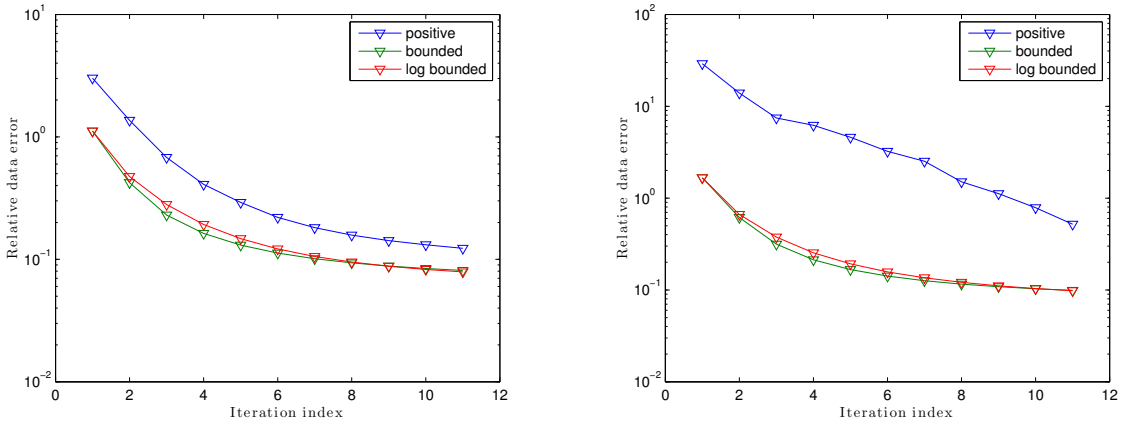

Figure 3. Left the data error reduction plots at each Gauss-Newton iteration for the three surrogate transformations in the 'high-variation' test. The corresponding error for the Tikhonov reconstruction was at 7×10^{-3}. To the right the corresponding curves for the 'low-contrast' test where the boundedness and logarithmic boundedness perform significantly better than the positiveness surrogate projected solution. In this case too the error of the Tikhonov solution was found to be 7×10^{-3}.

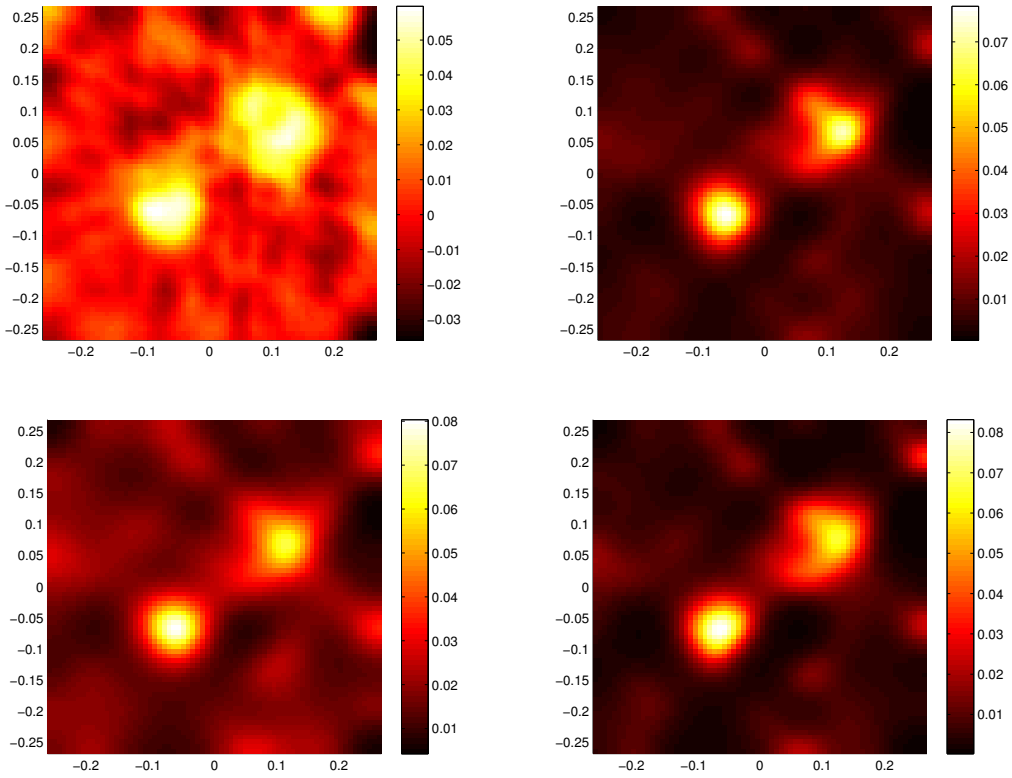

Figure 4. At the top row the high-dimensional Tikhonov solution and the image reconstruction with the positiveness surrogate. Below the corresponding images with boundedness and logarithmic boundedness constraints.

problem was then addressed using the Gauss-Newton algorithm and results from simulated and real measurements demonstrated that the spatial resolution of the images is significantly enhanced compared to Tikhonov-type solutions with smoothness imposing regularisation. Moreover, the results showed that bounding the image or its logarithm from below and above is critical in reconstructing plumes with low variation in their concentration profiles. The advantage of this is both quantitative and qualitative as the chemical concentration levels are recovered with better accuracy and at the same time the spatial resolution of the image is enhanced.

7. Acknowledgments

We kindly acknowledge the contribution of Walter Johnstone, Michael Lengden, David Wilson and Gordon Humphries of Strathclyde University for assisting in the experimental data acquisition as well as for providing the measurements used in this paper. We are also grateful to Victor Archilla and coworkers at INTA Madrid for facilitating the phantom tests. We also acknowledge EPSRC for funding this work in the context of FLITES : 'Fibre-Laser Imaging of gas Turbine Exhaust Species' project.

References

[1] Polydorides N, Tsekenis A, McCann H, Archilla V and Wright P 2016, *R. Soc. A* **472**, 2187
[2] Daun K J 2010, *J. Quant. Spectrosc. Radiat. Transf.* **111**, 105-115

[3] Bertsekas D P 1982, *SIAM J. Contr. Opt.* **20**(2), 221-246.
[4] Facchinei F, Júdice J and Soares J 1998, *SIAM J. Opt.* **8**(1), 158-186.
[5] Borsic A and Adler A 2012, *Inv. Prob.* **28**(9).
[6] Boyd S and Vandenberghe L 2004, Convex optimization, *Cambridge University Press*
[7] Commer M and Newman A G 2008, *Geophys. J. Int.* **172**, 513-535.
[8] Golub G H and Van Load C F 1996, Matrix Computations, *The John Hopkins Univ. Press*